Ruthenium-peptide conjugates for targeted phototherapy

Zhang, I.

2

Influence of the diimine spectator ligands on the photochemistry and anticancer properties of integrin-targeted macrocyclic ruthenium-peptide conjugates

*Targeting tumor cells or tumor vasculature using RGD-conjugated anticancer drugs is a recognized approach for cancer therapy due to the overexpression of integrins on the membrane of many types of cancer cells. In this work, three integrin-targeted macrocyclic ruthenium-peptide conjugates were synthesized by coordinating the two terminal histidine residues of the Ac-HRGDH-NH_2 pentapeptide to three different ruthenium(II) polypyridyl complexes. The corresponding conjugates, [Ru(bpy)$_2$(Ac-HRGDH-NH_2)]Cl_2 ([**1**]Cl_2, bpy = 2,2'-bipyridine), [Ru(dmbpy)$_2$(Ac-HRGDH-NH_2)]Cl_2 ([**2**]Cl_2, dmbpy = 6,6'-dimethyl-2,2'-bipyridine), and [Ru(Ph$_2$phen)$_2$(Ac-HRGDH-NH_2)]Cl_2 ([**3**]Cl_2, Ph$_2$phen = 4,7-diphenyl-1,10-phenanthroline) where synthesized and fully characterized. Photochemical studies showed that in water, upon green light activation [**1**]Cl_2 and [**3**]Cl_2 photodissociated only one of the histidine residues, while [**2**]Cl_2 released either one of the dmbpy chelates or the whole peptide. Monitoring the generation of singlet oxygen ($^1O_2$) and reactive oxygen species (ROS) showed that [**1**]Cl_2 and [**3**]Cl_2 demonstrate the characteristic properties of a photosensitizer for photodynamic therapy (PDT), while the sterically hindering dmbpy ligand in [**2**]Cl_2 generated a photoreactivity characteristic for photoactivated chemotherapy (PACT) compounds. In cytotoxicity studies, [**3**]Cl_2 showed the most promising anticancer properties, with photo index (PI) values up to 12 and EC_{50} ~2.5 μM under light irradiation in normoxia. Integrin $\alpha_v\beta_3$ expression and cellular uptake studies indicated these compounds to be taken up via a receptor-mediated process. Finally, based on their emissive properties, localization of conjugates [**1**]Cl_2 and [**3**]Cl_2 in cancer cells was studied by confocal laser scanning microscopy (CLSM), the results indicating that [**1**]Cl_2 mainly located in the lysosomes while [**3**]Cl_2 seemed to reside mainly in the Golgi area.*

This chapter will be submitted as a full paper: L. Zhang, G. Zhao, L. Bretin, Y. Husiev, A. Boyle, B. E. Snaar-Jagalska and S. Bonnet*, *manuscript in preparation*.

2.1 Introduction

Ruthenium-polypyridyl complexes are considered as promising metallodrugs and alternative candidates for cisplatin. To date, one Ru(II) compound (TLD1433) and three Ru(III) complexes (NAMI-A, KP1339 and BOLD-100) have progressed to clinical trials.[1] Due to the octahedral structure and attractive photophysical and photochemical properties, ruthenium(II) polypyridyl complexes can be designed in a controlled manner as photoactivatable drugs that may include multiple functional ligands. [2, 3] Photoactivation is a well-designed method to convert nontoxic prodrugs to active cytotoxic species in a spatially and temporally controlled manner.[4] This light-induced operation realizes "physical" tumor targeting by discriminating the light-irradiated malignant tumors from the non-irradiated healthy tissues, which can in principle reduce the dose-limiting side effects compared with standard chemotherapies.[5] Depending on the design strategy, two main photoactivation mechanisms can be implemented in ruthenium(II) polypyridyl complexes, called Photodynamic Therapy (PDT) and Photoactivated Chemotherapy (PACT). In PDT the photoreactive prodrug, called photosensitizer, combines with light and dioxygen to generate reactive oxygen species (ROS) in high concentrations that kill cancer cells, destroy blood vessels, and trigger immune antitumor response.[6, 7] In PACT, photosubstitution occurs instead, to generate in an oxygen-independent manner intermediates and/or photoproducts that can, individually or in combination, be more toxic to cells than the initial prodrug.[8-10]

Molecularly speaking, the distinction between PDT and PACT light activation mechanisms in ruthenium polypyridyl complexes is determined by the energy difference between the triplet metal-to-ligand-charge transfer (^{3}MLCT) excited states and the triplet metal-centered (^{3}MC) excited states of the metal complex. The lower the ^{3}MC state is, the faster a molecule will deactivate *via* photoinduced ligand dissociation, and thus generate a PACT effect. Different molecular design strategies were shown to be able to induce higher quantum yields for ligand photosubstitution, such as the introduction of ligands distorting the first coordination sphere by steric hindrance,[5, 11, 12] or increasing the lability of an Ru-L bond,[13] thus making a ruthenium complex a PACT prodrug. Though ruthenium-based anticancer drugs have been studied thoroughly and improved during the past decades, several issues still need to be addressed in the design of novel ruthenium(II) polypyridyl complexes for medicine, in particular to improve their selectivity, anticancer activity, and biocompatibility.[14] Besides the physical targeting allowed by light activation, advanced strategies that improve the tumor selectivity of a metal-based drug consist in using ligands bearing pendant chemical moieties such as small peptides

or vitamins, that can recognize specifically biomolecular targets.[14] This approach has been applied in diverse sub-fields of medicinal chemistry, especially using different cancer biomarkers as potential targets.[15, 16]

In this work, we report a series of three ruthenium-peptide cyclic conjugates, $[Ru(bpy)_2(Ac\text{-}HRGDH\text{-}NH_2)]^{2+}$ ([**1**]Cl_2, bpy = 2,2'-bipyridine), $[Ru(dmbpy)_2(Ac\text{-}HRGDH\text{-}NH_2)]^{2+}$ ([**2**]Cl_2, dmbpy = 6,6'-dimethyl-2,2'-bipyridine) and $[Ru(Ph_2phen)_2(Ac\text{-}HRGDH\text{-}NH_2)]^{2+}$ ([**3**]Cl_2, Ph_2phen = 4,7-diphenyl-1,10-phenanthroline), as candidates for integrin-targeted, photoactivated antitumor prodrugs. The small peptide Ac-HRGDH-NH_2 was designed based on the RGD sequence that is known to bind significantly to multiple integrin heterodimers, such as $\alpha_v\beta_1$, $\alpha_v\beta_3$, $\alpha_{IIb}\beta_3$ or $\alpha_v\beta_5$.[17] Integrins are transmembrane proteins that link the extracellular matrix with the cytoskeleton of cells and function as cell adhesion receptors.[18] RGD-binding integrins are involved in multiple cancer stages such as tumor growth, invasion, and metastasis,[19] which make them to be high potential targets especially for integrin-overexpressed types of cancer cells.[17, 20] The three ruthenium moieties $[Ru(bpy)_2(OH_2)_2]^{2+}$, $[Ru(dmbpy)_2(OH_2)_2]^{2+}$, and $[Ru(Ph_2phen)_2(OH_2)_2]^{2+}$ have been reported by several groups to be photoreleased when bound to different bidentate chelating ligands.[5, 21] Inspired by Fei et al.,[22] we considered using the Ac-HRGDH-NH_2 peptide as a protecting ligand for this family of ruthenium complexes, *i.e.*, to coordinate the two terminal histidine residues of the peptide to ruthenium, and observe how the resulting metal-peptide conjugate will react with visible light. With such a design, the RGD motif will be integrated into a cyclic structure, which has been reported to be beneficial to their selective interaction with integrins.[23]

The design is interesting for the development of anticancer PACT treatment for various reasons. First, although the use of peptides has emerged as an important approach for tumor-selective drug delivery, reports demonstrating the improved tumor targeting of ruthenium compounds by conjugation with peptides remain scarce.[14, 24, 25] Second, in most reported cases the peptide was attached covalently to one of the spectator ligands bound to ruthenium, rather than by direct coordination of amino-acid residues from the peptide to the metal center.[26, 27] If the ligand remains at all times bound to the ruthenium center, membrane binding of the conjugate does not necessarily allow to deliver the ruthenium load into the cells. Third, the conjugation of a peptide to a ruthenium-based PACT complex may enhance its potential as anticancer drug, as the peptide may increase the water-solubility, biocompatibility, and tumor selectivity of the metal complex. Last but not least, up to now it is unclear what (bis)histidine coordination would bring to the tris(bidentate) Ru(II) complex compared to (bis)pyridine, would it be easier to be

photosubstituted and turned to be PACT complex?[28, 29] In this work we report how histidine coordination influences the photochemistry and photoactivated therapy pathways of ruthenium-polypyridine complexes.

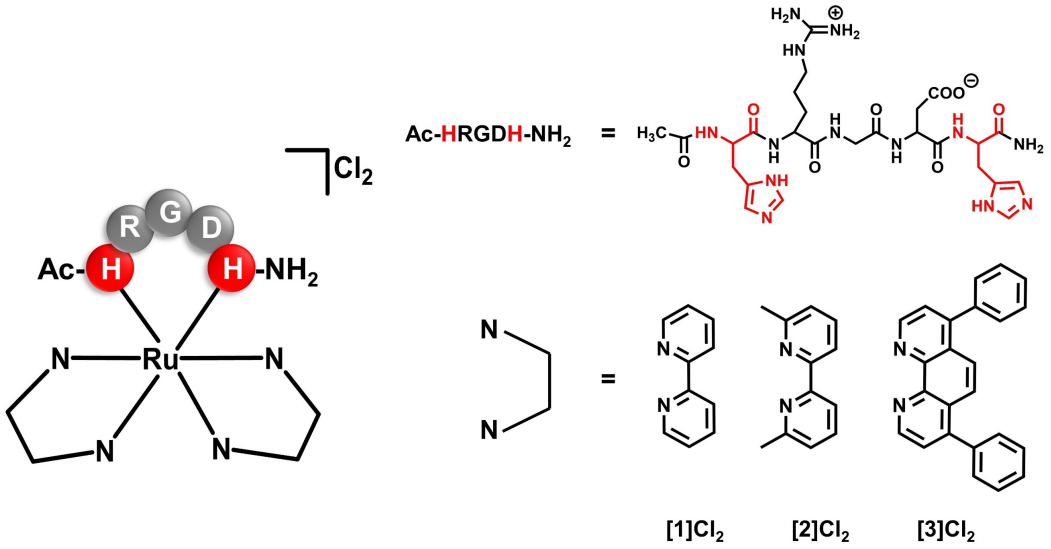

Scheme 2.1. *Chemical structures of the ligands and Ru-RGD conjugates [**1**]Cl_2, [**2**]Cl_2 and [**3**]Cl_2 studied in this work.*

2.2 Results

2.2.1 Synthesis and photochemical study

The Ru-RGD conjugates were synthesized by heating the racemic ruthenium precursor [Ru(bpy)$_2$Cl$_2$], [Ru(dmbpy)$_2$Cl$_2$] or [Ru(Ph$_2$phen)$_2$Cl$_2$] in presence of the peptide at pH=7.5 in mild conditions. For [**1**]Cl_2 the mixture was heated in water for 1 day at 90°C; for [**2**]Cl_2, 3 h at 60°C in water was enough to exchange the ligands, while for [**3**]Cl_2 the higher lipophilicity of the dpp ligand required a 1:1 ethanol : water mixture and 1 day at 90°C under N_2 to realize coordination. All complexes were purified by preparative HPLC. The coordination of two histidines from one peptide to one ruthenium center was confirmed successful by NMR, mass spectra (MS) and high-performance liquid chromatography (HPLC) (Figure AII.1-8). For example: the ratio of Ru:Ph$_2$phen:peptide = 1:2:1 in [**3**]Cl_2 was confirmed by MS without other ligand involved, with single peaks detected in HPLC and shift of the four protons from two imidazoles of peptide after coordination. Log P measurements were performed to characterize the influence of the peptide and of the spectator diamine ligands on lipophilicity. As shown in Table AII.1, the lipophilicity gradually increases from [**1**]Cl_2 to [**2**]Cl_2 to [**3**]Cl_2, while both control complexes [Ru(bpy)$_3$]Cl_2 and [Ru(Ph$_2$phen)$_2$(bpy)]Cl_2 are more lipophilic than the

peptide-coordinated conjugates [**1**]Cl_2 and [**3**]Cl_2, respectively. Overall, peptide conjugation increases significantly the water solubility of the ruthenium complexes.

To characterize the photosubstitution properties of **[1]**Cl_2-**[3]**Cl_2, the evolution of their absorption spectra with time under 515 nm green light irradiation was first monitored in pure H_2O (Figure 2.1). The spectrum of [**1**]Cl_2 showed limited changes upon light irradiation (Figure 2.1a), which could be the consequence either of a good photostability, or of a photoproduct that possesses an absorption spectrum similar to that of [**1**]Cl_2. Unexpectedly, upon excitation at 480 nm [**1**]Cl_2 showed significant emission in the 600-800 nm region (Figure AII.9a). Monitoring the emission spectrum during continuous 515 nm green light irradiation demonstrated that emission decreased gradually, suggesting that the original conjugate [**1**]Cl_2 may indeed be photo-labile. In the mass spectrum (MS) of the mixture after irradiation (515 nm, 4.0 mW/cm^2, 2 h, Figure AII.11a), a new peak at *m/z* = 372.6 appeared, which corresponds to $\{[Ru(bpy)_2(\eta^1\text{-Ac-HRGDH-NH}_2)(H_2O)]+Na\}^{3+}$, suggesting that one Ru-His bond was photolabilized and the histidine ligand substituted by H_2O. Combining both observations, we conclude that green light induces photosubstitution of one of the histidines of the peptide in pure H_2O. Since water is not a good ligand for ruthenium(II), the photosubstitution study was repeated in an aqueous solution containing 50 vol% acetonitrile. As shown in Figure AII.10a, the spectra showed more apparent changes, compared to that observed in pure water, confirming that the minimal spectroscopic changes upon irradiation in pure water can be ascribed to the similar absorption spectra of the reagent and product. MS analysis of the irradiated 1:1 v/v H_2O:MeCN solution showed a peak at *m/z* = 247.6, corresponding to $[Ru(bpy)(MeCN)_2]^{2+}$ (Figure AII.11b), confirming that in these conditions the peptide was released and photosubstituted by two acetonitrile ligands. Overall, [**1**]Cl_2 was found to be photosubstitutionally active, but in pure water the reaction is slow, leading in our irradiation conditions to the photosubstitution of a single histidine, while in presence of significant amounts of the better ligand acetonitrile, both histidines are substituted.

In principle, methyl groups *ortho* to the nitrogen atoms of a bipyridine ligand coordinated to ruthenium increase the steric strain of the complex, which leads to a strong alteration of its photochemistry.[12, 30, 31] For [**2**]Cl_2, in which the spectator 2,2'-bipyridine ligand of [**1**]Cl_2 is replaced by 6,6'-dimethyl-2,2'-bipyridine, a significant acceleration of the photosubstitution reaction in pure water was observed (Figure 2.1b). The changes in the absorption spectra, characterized by an increase of the absorbance at 497 nm, levelled off after 20 min irradiation (515 nm, 4.0 mW/cm^2, 2 h). A mass spectrum taken after irradiation showed peaks at *m/z* =

275.9 and 515.1, which correspond to the photoproducts $[Ru(dmbpy)_2(H_2O)_2]^{2+}$ and $[Ru(dmbpy)(\eta^1\text{-Ac-HRGDH-NH}_2)(H_2O)_2]^{2+}$, respectively. Thus, two photosubstitution reactions took place in parallel: either the peptide or one dmbpy ligand was released (Figure AII.12a). When a stronger donor was present in the solvent, *i.e.,* when irradiation was performed in 1:1 v/v H_2O:MeCN (Figure AII.10b), decrease of the absorbance at 497 nm was observed and only $[Ru(dmbpy)(Ac\text{-HRGDH-NH}_2)(MeCN)_2]^{2+}$ was detected in the mass spectra (*m/z* = 268.0, Figure AII.12b). As a consequence, in these conditions one dmbpy ligand is selectively replaced by two MeCN molecules upon light activation. Unlike for [**1**]Cl_2, no phosphorescence was observed when [**2**]Cl_2 was excited at λ=480 nm in water (Figure AII.9b). The ligand 4,7-diphenyl-1,10-phenanthroline (Ph_2phen) in [**3**]Cl_2 is more lipophilic than bpy but also non-hindered. From the evolution of the UV-vis and emission spectra of [**3**]Cl_2 in H_2O (Figure 2.1c and AII.9c), the photochemistry of [**3**]Cl_2 was found to be quite similar to that of [**1**]Cl_2: in aqueous conditions only one histidine was photosubstituted by water, and the photoreaction was still going on at the end of our 2 h irradiation time (515 nm, 4.0 mW/cm^2, see Figure AII.12a). When [**3**]Cl_2 was irradiated in presence of acetonitrile, the absorbance spectra shifted hypsochromically, and the formation of $[Ru(Ph_2Phen)(MeCN)_2]^{2+}$ was confirmed by MS (Figure AII.13b). From the above studies it appears that the Ru-peptide conjugates [**1**]Cl_2 and [**3**]Cl_2 undergo slow photosubstitution in weakly coordinating solvents such as H_2O, and only one Ru-His bond is broken after 2 h irradiation in such conditions. In solvents with stronger coordination properties (MeCN), two Ru-His bonds are cleaved upon irradiation, leading to peptide release. By contrast, the sterically hindered conjugate [**2**]Cl_2 is more labile already in pure H_2O, where it releases in parallel either the peptide or the dmbpy ligand.

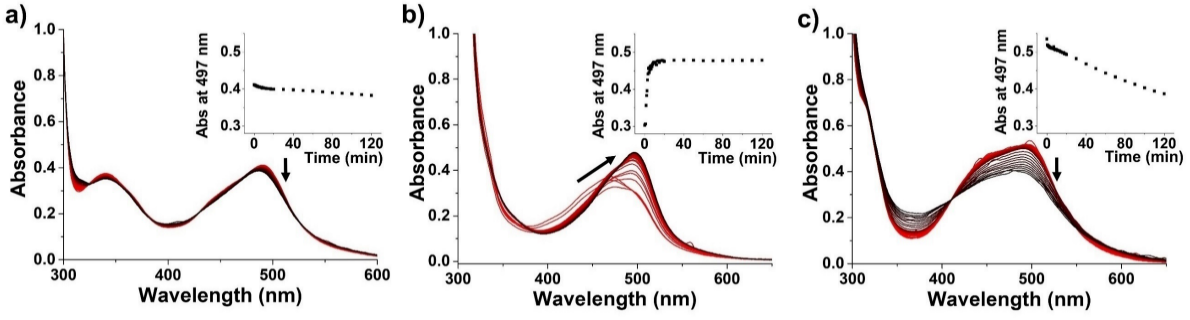

Figure 2.1. *Evolution of the UV-vis spectra of conjugates [**1**]Cl_2 (a, 70 μM), [**2**]Cl_2 (b, 67 μM) and [**3**]Cl_2 (c, 60 μM) in H_2O upon 515 nm LED irradiation (4.0 mW/cm^2, 120 min). Inset: time evolution of the absorbance of the solution at 497 nm.*

2.2.2 In vitro cytotoxic study

To determine the potency of the Ru-peptide conjugates as photo-activatable metallodrugs, their cytotoxicity was measured in A549 and MCF7 human cancer cell lines both under normoxic (21% O_2) and hypoxic (1% O_2) conditions. Hypoxia is a characteristic hallmark of solid tumors. It comes as a consequence of the high consumption of oxygen by cancer cells and inefficient oxygen delivery in tumors,[32] and it is associated with different kinds of resistances to a number of anticancer agents, especially (but not only) PDT drugs.[33] Here, cells were treated with [**1**]Cl_2, [**2**]Cl_2, or [**3**]Cl_2 for 24 h, after which green light (520 nm, normoxia, 10.92 mW/cm^2, 13.1 J/cm^2, 20 min; hypoxia 520 nm, 7.22 mW/cm^2, 13.1 J/cm^2, 30 min) was applied. A second plate was left non-irradiated as dark control. After 48 h further incubation in the dark, the relative cell population in each well was determined by a sulforhodamine (SRB) assay, and the cytotoxicity of the complexes was quantified by determination of the half-maximal effective concentrations (EC_{50} in μM, defined as the concentration that was able to kill half of the cancer cells, compared to untreated wells) and the photoindex values (PI = $EC_{50,dark}/EC_{50,light}$). The cell viability curves are shown in Figure AII.14 (A549) and AII.15 (MCF7), and the corresponding EC_{50} values are summarized in Table 2.1. According to these data, [**1**]Cl_2 showed weak cytotoxicity towards any of the cell lines (< 100 μM), both under normoxia and hypoxia. In normoxic A549, photoactivated cytotoxicity was only observed at high concentrations (>150 μM). [**2**]Cl_2, by contrast, showed better performance with PI values in normoxic A549 and MCF7 cells of 4.4 and 2.3, respectively. In hypoxic conditions, both $EC_{50,dark}$ and $EC_{50,light}$ increased, which is a good illustration of the known resistance of hypoxic cells towards chemotherapy; the resulting PI value (2.3) was lower than under normoxia (4.4). The limited phototoxicity of [**2**]Cl_2 might come from 1) the thermal instability of the conjugate in medium (Figure AII.16b), which may artificially decrease the $EC_{50,dark}$ values, 2) the low cytotoxicity of the photoproduct, either dmbpy, $[Ru(dmbpy)_2(H_2O)]^{2+}$, or $[Ru(dmbpy)(Ac\text{-}HRGDH\text{-}NH_2)(OH_2)_2]^{2+}$, or 3) a combination of both effects. The high steric hindrance of the two possible ruthenium-containing photoproducts may hamper binding to biological ligands such as DNA or proteins, thus lowering toxicity after activation. Compound [**3**]Cl_2 showed the highest phototoxicity. For normoxia A549 and MCF7 cells, the EC_{50} values in the dark was ~30 μM, while after light irradiation the values decreased to 2.5 μM for A549 and 4.2 μM for MCF7, giving a PI value of 12 and 7.1, respectively. Considering its photosubstitution behavior in MeCN/H_2O, such promising PI values in normoxia implies that conjugate [**3**]Cl_2 might be a potential candidate for PACT. Unfortunately, however, in hypoxic A549 cells, [**3**]Cl_2 didn't

show high toxicity upon irradiation: though the $EC_{50,dark}$ (40 μM) was comparable to that in normoxia (30 μM), the $EC_{50,light}$ was almost one order of magnitude higher, thus leading to a low PI of 1.4. According to the above data, the anticancer properties of the three conjugates is strongly influenced by the chemical nature of the bisimine chelating ligands. [**3**]Cl_2 showed the best light activation in normoxia, but its poor performance in hypoxia suggests that its phototoxicity may be O_2-dependent for reasons yet to be determined. Upon replacement of the lipophilic but non-hindered Ph_2phen ligands by the sterically hindering but less hydrophobic dmbpy ligands, lower PI values were obtained for [**2**]Cl_2 in normoxia, but the PI remained higher than 1 under hypoxia, suggesting at least a partial PACT mechanism operative. Finally, [**1**]Cl_2 appeared to be non-toxic in all tested conditions, suggesting either that the complex does not enter the cells, or that the photoproduct e.g. $[Ru(bpy)_2(OH_2)(\eta^1\text{-Ac-HRGDH-NH}_2)]^{2+}$ is simply not toxic enough.

Table 2.1. *Half-maximal effective concentrations (EC_{50} in μM) of conjugates [**1**]Cl_2, [**2**]Cl_2 and [**3**]Cl_2 in the dark and upon green light activation in 2D cancer cell monolayers under normoxic (21% O_2) or hypoxic (1% O_2) conditions.* [a, b, c]

Cell lines	[1]Cl_2			[2]Cl_2			[3]Cl_2		
	$EC_{50,dark}$ (μM)	$EC_{50,light}$ (μM)	PI	$EC_{50,dark}$ (μM)	$EC_{50,light}$ (μM)	PI	$EC_{50,dark}$ (μM)	$EC_{50,light}$ (μM)	PI
A549 (Normoxia)	>100	>100	/	88 +17 -14	24 +6 -5	**4.4**	30 +5 -4	2.5 +0.5 -0.5	**12**
MCF7 (Normoxia)	>100	>100	/	83 +6 -5	42 +6 -5	**2.0**	30 +4 -4	4.2 +1.0 -0.8	**7.1**
A549 (Hypoxia)	>100	>100	/	162 +>100 -32	70 +10 -9	**2.3**	40 +18 -8	28 +4 -4	**1.4**

[a] *95% confidence interval (CI in μM) and photoindexes ($PI = EC_{50,dark}/EC_{50,light}$) are also indicated.* [b] *Irradiation conditions: 520 nm, 10.92 mW/cm², 13.1 J/cm², 20 min under normoxia; 520 nm, 7.22 mW/cm², 13.1 J/cm², 30 min under hypoxia.* [c] *Cancer cells were treated for 24 h (=DLI) without any washing before light activation.*

2.2.3 Photoactivated pathways

In PDT and PACT the toxic substances produced upon light activation are fundamentally different. PDT photosensitizers generate reactive oxygen species (ROS) through energy transfer or electron transfer, and both paths are oxygen-dependent. In contrast, PACT prodrugs do not

require oxygen to become phototoxic,[34] but release toxic species through photochemical reactions, either as ligands,[9] ruthenium complexes,[35] or both.[36] To address which pathways is active in the Ru-peptide conjugates [**1**]Cl_2-[**3**]Cl_2, singlet oxygen ($^1O_2$) generation quantum yields (Φ_Δ) were firstly measured for all three compounds. The Φ_Δ values of the three conjugates were measured by direct detection of the 1274 nm infrared emission from $^1O_2$ under 450 nm excitation in CD_3OD (Figure AII.17).[37] The prototypical [Ru(bpy)$_3$]Cl_2 complex was used as a reference (Φ^{ref} =0.73). [**2**]Cl_2 has a Φ_Δ value of 0.03 (Table AII.2), which corresponds to a low level of $^1O_2$ generation. On the other hand, the Φ_Δ values of [**1**]Cl_2 and [**3**]Cl_2 are 0.19 and 0.26, respectively, which represents a significant level of $^1O_2$ generation. Both complexes are hence potential PDT agents.

Next, intracellular reactive oxygen species (ROS) measurements were accomplished using a deep red ROS molecular probe. To do so, A549 cells were first treated with the ruthenium conjugates (15 μM) for 24 h, the medium was then replaced with drug-free medium, and the cells were further kept in the dark or irradiated with green light (515 nm, 13.1 J/cm^2). Then, the cells were cultured with the ROS indicator (Cellular ROS Assay Kit, Deep Red, ab186029). Finally, flow cytometry was used to determine the amount of ROS produced in the treated cells (Figure AII.18). The mean fluorescence intensity was chosen as quantification (Table AII.3). Rose Bengal was used as a PDT type II control, and tBHP (*tert*-butyl hydroperoxide) was taken as positive control for radical generation. As shown in Table AII.3, the ROS production intensity ratio between irradiated and dark conditions was 2.43 for Rose Bengal. For [**1**]Cl_2 and [**2**]Cl_2 barely any difference could be measured between dark and light conditions, which suggested that intracellular ROS generation did not take place for these compounds. For complex [**2**]Cl_2 this result fits well with the low $^1O_2$ generation quantum yield, while for [**1**]Cl_2 the low ROS generation must be due to poor uptake, as the $^1O_2$ generation quantum yield was significant. Compound [**3**]Cl_2, on the other hand, showed a dramatically higher ROS generation upon light irradiation even compared to Rose Bengal (ratio 6.52), which fits with its comparatively good Φ_Δ values (0.26). Overall, we conclude from these experiments that [**3**]Cl_2 is essentially a PDT agent and not a PACT agent, as it generates significant amounts of ROS and $^1O_2$, and it has poor photoactivated cytotoxicity in hypoxia. Considering its similar photochemistry, [**1**]Cl_2 should behave like [**3**]Cl_2, but its poor lipophilicity may critically prevent crossing the cell membrane. Finally, the phototoxicity observed for [**2**]Cl_2 must be the result of ligand dissociation, suggesting a PACT pathway for this compound, although its instability in cell culture medium probably explains the comparatively low PI values.

2.2.4 Cellular uptake

To better understand the difference in efficacy of compounds [**1**]Cl_2-[**3**]Cl_2 between different human cancer cell lines, as well as between cells grown in normoxia and cells grown under hypoxia, a cellular metal-uptake study was conducted. A549 lung cancer cells have been reported to have higher integrin expression levels than MCF7 cells, which have comparatively low integrin expression.[38] To check this reported difference, we first quantified the integrin $\alpha_v\beta_3$ expression level at the surface of A549 and MCF7 cells that had been cultured either at 21% or 1% O_2 for more than a month. Using a reported double-immunofluorescence protocol,[39] cells were collected and incubated first with anti-integrin $\alpha_V\beta_3$ antibody, then with Alexa Fluor™ 488 conjugated goat anti-mouse IgG secondary antibody. The integrin $\alpha_V\beta_3$ expression levels were finally analyzed with flow cytometry. Negative control consisted of cells only incubated with the secondary antibody. The results are shown in Figure 2.2a and the quantification (mean florescence-intensity values) is summarized in Table AII.4. First, normoxic or hypoxic MCF7 cells showed very low mean fluorescence intensity (1575 and 1671 for normoxia and hypoxia, respectively), compared to control (2571 in normoxia, 1247 in hypoxia), which means that MCF7 cells have low integrin $\alpha_v\beta_3$ expression. A549 cells, by contrast, expressed integrin $\alpha_v\beta_3$ at a much higher levels, especially in hypoxic conditions (mean cell-fluorescence intensity of 7249 and 14176 for normoxia and hypoxia, respectively). Hypoxic cells have been reported to upregulate many cellular processes to respond to the O_2 shortage.[15] It is interesting to note that higher integrin $\alpha_v\beta_3$ expression is part of the pathways upregulated in hypoxic A549 cells, which suggested that cyclic RGD-ruthenium conjugates could offer new perspectives to overcome the resistance induced by hypoxia.

In a second step, experiments for cellular uptake of the conjugates were conducted. A549 and MCF7 cells cultured in normoxic or hypoxic conditions were treated with one of the conjugates (20 μM) for 24 h. After washing with drug-free medium, the cells were collected and counted, and their ruthenium content was determined with inductively coupled plasma mass spectrometry (ICP-MS). Cells treated with drug-free medium were used as negative control, and the ruthenium complexes $[Ru(bpy)_3]Cl_2$ and $[Ru(Ph_2phen)_2(bpy)]Cl_2$ were also involved in the study for comparison. The cellular uptake values are summarized in Table AII.5. According to these data, the ruthenium accumulation of [**1**]Cl_2 is the lowest among all three conjugates in most of the cell lines. As discussed before, the low cytotoxicity of compound [**1**]Cl_2 may be caused by the low cellular uptake, the wrong intracellular localization, or simply a low toxicity. The low cellular uptake efficiency of [**1**]Cl_2 was confirmed at least to be one of the explanation.

The highest uptake for [**3**]Cl_2 in all cells and conditions, highlighting the higher lipophilicity of this compound due to the Ph_2phen ligands. When comparing cell lines, the data for the three conjugates showed that A549 cells exhibited significant higher Ru accumulation than the MCF7 cells, which fits with the amount of integrin expression. For example, the Ru content of conjugate [**3**]Cl_2 in normoxic A549 cells was found to be 1.24 ± 0.11 μg Ru/million cells, while in normoxic MCF7 cells, the value was 0.80 ± 0.07 μg Ru/million cells. However, this variation was not observed in the two control compounds [Ru(bpy)$_3$]Cl_2 and [Ru(Ph_2phen)$_2$(bpy)]Cl_2 not containing an RGD peptide. After peptide conjugation, the intracellular accumulation of the ruthenium complex was efficiently improved, for example, the Ru content of [Ru(Ph_2phen)$_2$(bpy)]Cl_2 in hypoxic A549 was 0.59 ± 0.12 μg Ru/million cells, while for [**3**]Cl_2 , it was increased to 2.20 ± 0.15 μg Ru/million cells. As expected, the conjugates also showed even higher uptake in hypoxic cells, especially for conjugate [**3**]Cl_2, for which a dramatic increase of the Ru uptake was found (1.24 ± 0.11 *vs.* 2.20 ± 0.15 μg/million cells for normoxia *vs*. hypoxia, respectively).

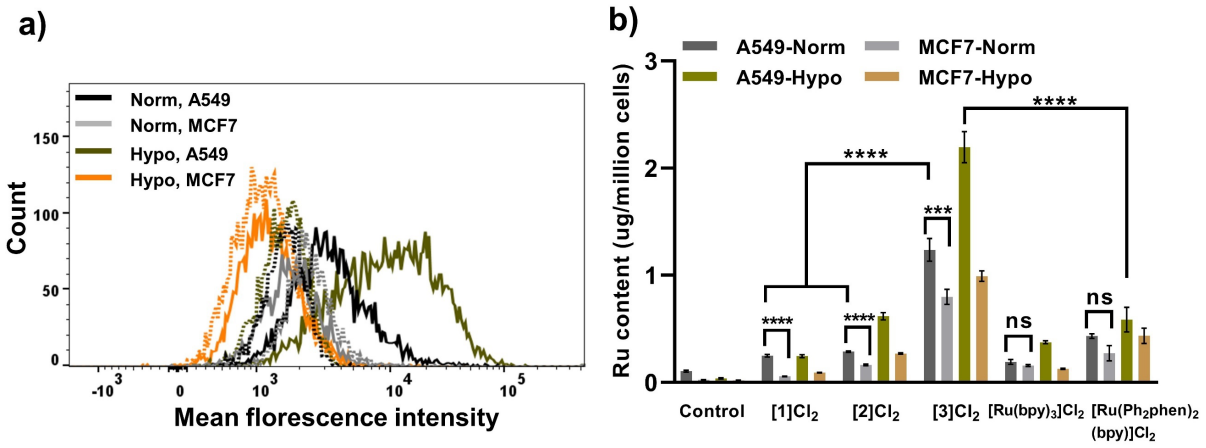

Figure 2.2. *a) Representative flow cytometry histogram of integrin $a_V\beta_3$ expression in A549 and MCF7 human cancer lines in normoxic (21% O_2) and hypoxic (1% O_2) conditions. Solid lines represent the fluorescence intensity of the cells after incubation with anti-integrin $a_V\beta_3$ first antibody, followed by Alexa Fluor™ 488 conjugated goat anti-mouse IgG second antibody. Dotted lines indicate the background staining with only secondary antibody. b) Ru accumulation in A549 and MCF7 cells after exposure to vehicle control, [**1**]Cl_2, [**2**]Cl_2, [**3**]Cl_2, [Ru(bpy)$_3$]Cl_2 or [Ru(Ph_2phen)$_2$(bpy)]Cl_2 (20 μM, dark) for 24 h under normoxia and hypoxia. Every group was conducted by sextuplicate wells, and errors were determined by standard error of the mean (SEM). Unpaired t-test was used to determine the significance of the comparisons of data indicated in b (*P < 0.05; **P < 0.01; ***P < 0.001; ****P < 0.0001).*

2.2.5 Localization study

Efficient cellular uptake is a must for most drugs, but the ability of the drug to localize into specific subcellular organelles is also important, as it determines how the drug molecules may interact with cancer cells. As [**1**]Cl_2 and [**3**]Cl_2 are emissive upon excitation at 480 nm, localization of these compounds within the cell was investigated using confocal microscopy. A549 cells were treated with [**1**]Cl_2 (100 μM) or [**3**]Cl_2 (20 μM) for 3 h, and after medium refreshing the cells were imaged with confocal microscopy. Deep red luminescence (Figure AII.19 and 20) observed inside the cells clearly demonstrated cellular uptake of both Ru-peptide conjugates. Further colocalization study was conducted with four commercial organelle dyes, *i.e.* Nuclear Blue, Mito tracker green, Lyso tracker green and Golgi tracker green for nuclei, mitochondria, lysosome, and Golgi localization, respectively. As shown in Figure 2.3 for [**3**]Cl_2 and Figure AII.21 for [**1**]Cl_2, the confocal images showed nuclear accumulation for neither compound. Pearson's correlation coefficients (PCC) were calculated for each organelle based on the degree of overlapping between emission from the commercial dye (GFP) channel and that of the complex (deep red) channel. The results for the region-of-interest (ROI) images are summarized in Table AII.6. A PCC value higher than +0.5 represents a strong positive correlation, while PCC values between +0.3 and +0.5 represent medium co-localization, PCC values lower than +0.3 mean low co-locolization, and negative values represent anti-correlation. Compound [**1**]Cl_2 (Figure AII.21 and Table AII.6) showed strong correlation with Lyso tracker (PCC = +0.58), while for Mito tracker and Golgi tracker the overlapping levels were weak, indicating that [**1**]Cl_2 mainly located in the lysosomes. By contrast, for [**3**]Cl_2 (Figure 2.3) the highest PCC value was found with the Golgi tracker (PCC = +0.39), followed with Mito tracker (PCC = +0.18). The Lyso tracker showed negative correlation (PCC = -0.25). Overall, [**3**]Cl_2 was mostly found in the Golgi area as well as in other non-identified regions of the cells.

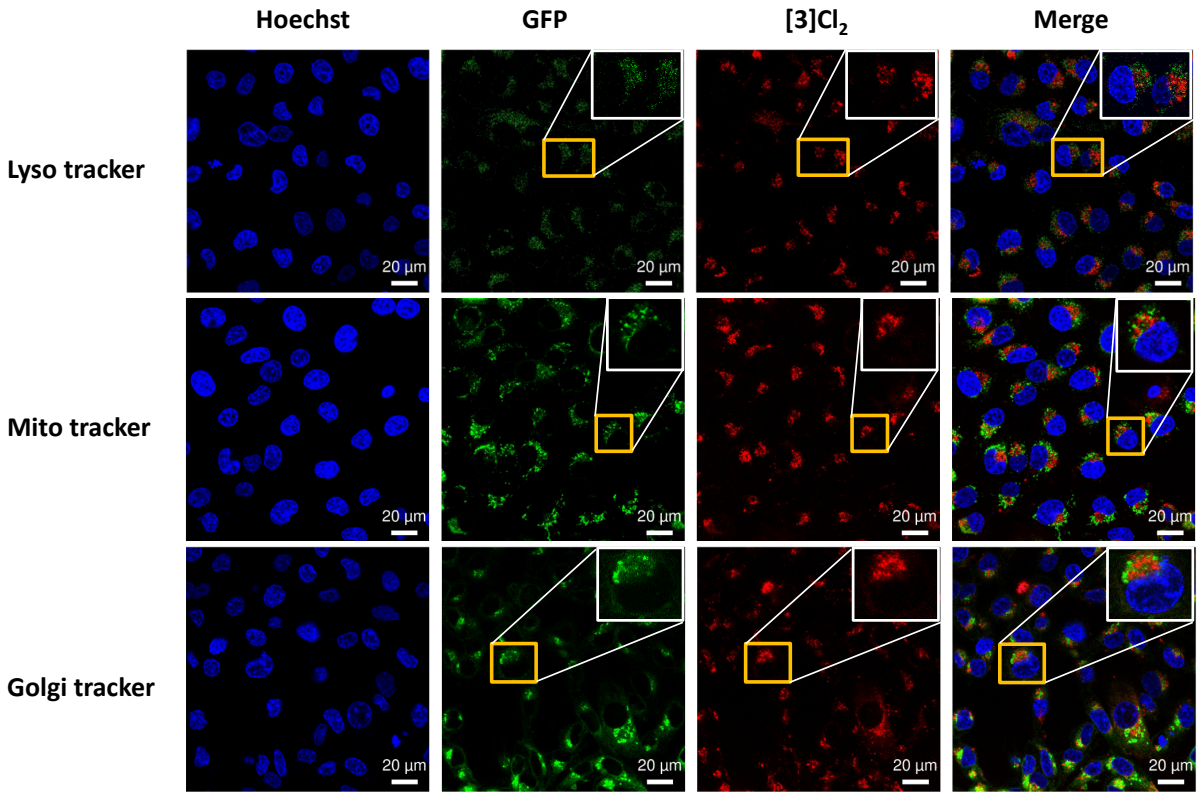

Figure 2.3. *Confocal microscopy images of A549 cells co-treated with [**3**]Cl_2 (20 µM for 3 h), Hoechst (30 min), and either Lyso tracker green (100 nM for 1 h), Mito tracker green (20 nM for 1 h) or Goigi tracker green (20 nM for 1 h). The ROI used for the calculation of the Pearson correlation coefficients (PCC, Table AII.6) are shown as insets. Scale bar is 20 µm.*

2.3 Discussion

As shown in this work, RGD peptide conjugation to ruthenium-polypyridyl complexes serves to improve their water solubility and at the same time their uptake in cancer cells. However, comparing log-P data to cellular uptake (Figure 2.2b and Table AII.4) suggests that cellular uptake is influenced not only by interaction with integrin receptors, but also by lipophilicity of the compounds. Within the series of Ru-peptide conjugates [**1**]Cl_2-[**3**]Cl_2, more lipophilic bis-imine ligands improved cellular uptake after 24 h dark incubation. As they all have the same integrin-targeting peptide, passive uptake must take place at least partially. On the other hand, [Ru(Ph_2phen)$_2$(bpy)]Cl_2, showed less Ru accumulation within the cells than [**3**]Cl_2, while it is significantly more hydrophobic (log P: +0.82 *vs.* +0.11). These observations indicate that the replacement of a bpy ligand by the Ac-HRGDH-NH_2 pentapeptide increased the hydrophilicity of the Ru complex, but on the other hand introduced active targeting of the cells. Overall, when considering the integrin expression of the different cell lines, the uptake study, and the log P measurements, we can reasonably conclude that receptor-mediated uptake is taking place *in*

vitro for Ru-peptide conjugates [**1**]Cl_2-[**3**]Cl_2, highlighting their potential as metallodrugs capable of targeting $\alpha_v\beta_3$ integrin-overexpressing tumors.

Coordination of two histidines to the non-hindered ruthenium fragments [Ru(bpy)$_2$] or [Ru(Ph$_2$phen)$_2$] did not generate PACT complexes, but surprisingly resulted in PDT complexes. It appeared to be necessary to introduce significant steric hindrance, such as with dmbpy, to transform the PDT complex [**1**]Cl_2 into the PACT compound [**2**]Cl_2. On the other hand, [**2**]Cl_2 was shown to be not very stable in cell-culture medium in the dark, which lowers its potential as real PACT prodrug. When designing new ruthenium-peptide PACT conjugates in the future, a better balance should be found between steric hindrance and photoactivity, to achieve both a good dark stability and high photosubstitution efficiency.

2.4 Conclusion

Three HRGDH-based ruthenium(II) polypridine complexes were successfully synthesized with different bis-imine chelates. Their photochemistry and cellular behavior were strongly influenced by the structure of the bis-imine ligands. With bpy ([**1**]Cl_2) and Ph$_2$phen ([**3**]Cl_2) chelating ligands, PDT compounds were obtained that generated both $^1O_2$ and phosphorescence upon irradiation. Use of sterically hindering dmbpy ligands turned the ruthenium complex into a PACT compound ([**2**]Cl_2). According to the integrin $\alpha_v\beta_3$ expression and uptake studies, integrin receptor-mediated cellular uptake took place with these compounds, which we interpret as a consequence of the RGD component of the pentapeptide. Colocalization studies suggested that [**1**]Cl_2 mainly located in the lysosomes and [**3**]Cl_2 in the Golgi area. Overall, [**3**]Cl_2 was found to be the most promising prodrug, that had appealing phototoxicity and high uptake efficiency. In conclusion, the coordination of metal-binding peptides such as Ac-HRGDH-NH_2 appears to be an effective tool to improve the biocompatibility, uptake efficiency, and specific cancer-cell targeting of ruthenium-polypyridyl complexes. We hope this work provides a basis for photoactive ruthenium complexes to conjugate with functional proteins, such as monoclonal antibodies for active tumor targeting in the future.[40, 41]

2.5 Experimental section

The cytotoxicity assays (2D), integrin expression, log P determination and measurement of intracellular ROS were carried out according to the methods described in Appendix I.

2.5.1 Synthesis

2.5.1.1 General

cis-Bis(2,2′-bipyridine)dichloridoruthenium(II) hydrate (*cis*-[Ru(bpy)$_2$Cl$_2$]), the ligands 6,6'-dimethyl-2,2'-bipyridine and 4,7-diphenyl-1,10-phenanthroline as well as RuCl$_3$·3H$_2$O were purchased from Sigma-Aldrich. Lithium chloride (LiCl) was purchased from Alfa-Aesar. The amino acids Fmoc-His(Trt)-OH, Fmoc-Arg(Pbf)-OH, Fmoc-Gly-OH, and Fmoc-Asp(OtBu)-OH for peptide synthesis were purchased from Merck Millipore. All reactants and solvents were used without further purification. *cis*-[Ru(dmbpy)$_2$Cl$_2$], *cis*-[Ru(Ph$_2$phen)$_2$Cl$_2$] and [Ru(Ph$_2$phen)$_2$(bpy)]Cl$_2$ were synthesized according to literature procedures.[5, 42]

2.5.1.2 Ac-HRGDH-NH$_2$

The peptide was synthesized on a CEM Liberty microwave synthesizer, according to standard Fmoc solid-phase protocols. The peptides were synthesized from their C-termini to N-termini. The acetylation of N-termini was realized by 1:1:3 acetic anhybride/pyridine/DMF reacting for 1 h. After cleavage from the resin (95% TFA : 2.5% H$_2$O : 2.5% Tis), the collected peptides were precipitated with cold ethyl ether, stored at 4°C for 3 h and then washed 3 times by cold diethyl ether (3×30 mL). The peptide was then dissolved in MilliQ water (10 mL) and lyophilized for further LC-MS test. The peptide purity was >90%, thus it was used for conjugation to ruthenium without further purification.

2.5.1.3 [Ru(bpy)$_2$(Ac-HRGDH-NH$_2$)]Cl$_2$ ([1]Cl$_2$)

cis-Ru(bpy)$_2$Cl$_2$ ·2H$_2$O (0.05 mmol, 26 mg) was added to a 2-neck 25 ml flask, the flask was vacuum-flushed with N$_2$ 3 times, deoxygenated MilliQ H$_2$O (3 mL) was added and the ruthenium solution was stirred at 90°C for 10 min. The peptide Ac-HRGDH-NH$_2$ (0.05mmol, 33 mg) was dissolved in MilliQ water (3 mL) and the pH adjusted to 7.5 by 0.5 mM and 0.1 mM NaOH and HCl solution. The peptide solution was deaerated by bubbling N$_2$ for 10 min and then injected to the reaction flask . The mixture was then stirred at 90°C for 1 day. After that, the solution was cooled down to room temperature and lyophilized, to afford a reddish powder. Further purification was accomplished by HPLC. The purification was realized by a 250 x 21.2 mm Jupiter® 4 µm Proteo 90 Å C12 column using Thermo Scientific UHPLC system. The gradient was controlled by four pumps. The mobile phase consisted in H$_2$O containing 0.1% v/v trifluoroacetic acid (TFA) (A phase) and acetonitrile containing 0.1% v/v Trifluoroacetic acid (TFA) (B phase). The gradient for preparative separation of [**1**]Cl$_2$ was 10-20% MeCN/H$_2$O for 20 min. The fractions were monitored by four UV detector (214 nm, 290

nm, 350 nm, 450 nm) and the flow rate was 14 mL/min. The compound was collected at UV-detector 290 nm. [**1**]Cl_2, ESI-MS: (calc. *m/z* for $[\mathbf{1}]^{2+}$ = 537.5 and $[\mathbf{1}]^{3+}$ = 358.3), found: 537.5 and 359.0, HPLC (10-90% MeCN/H_2O with 0.1% TFA, 20 min): t_R = 8.9 min.

2.5.1.4 [Ru(dmbpy)$_2$(Ac-HRGDH-NH$_2$)]Cl$_2$ ([2]Cl$_2$)

cis-Ru(dmbpy)$_2$Cl$_2$ (0.05 mmol, 27 mg) was added to a 2-neck 25 ml flask, the flask was vacuum-flushed with N_2 3 times, deoxygenated MilliQ H_2O (3 mL) was added and the ruthenium solution was stirred at 90°C for 10 min. The peptide powder Ac-HRGDH-NH_2 (0.05mmol, 33 mg) was dissolved in MilliQ water (3 mL) and the pH adjusted to 7.5 by 0.5 mM and 0.1 mM NaOH and HCl solution. The peptide solution was deaerated by bubbling N_2 for 10 min and then injected to the reaction flask . The mixture was then stirred at 90°C for 1 day. After that, the solution was cooled down to room temperature and lyophilized, to afford a reddish powder. Further purification was accomplished by HPLC. The purification were realized by a 250 x 21.2 mm Jupiter® 4 µm Proteo 90 Å C12 column using Thermo Scientific UHPLC system. The gradient was controlled by four pump. Mobile phase consisted H_2O containing 0.1% v/v formic acid (A phase) and acetonitrile containing 0.1% v/v formic acid (B phase). The gradient for [**2**]Cl_2 preparative separation was 10-20% MeCN/H_2O for 20 min. The analysts were monitored by four UV detector (214 nm, 290 nm, 350 nm, 450 nm) and the flow rate was 14 mL/min. Compound were collected at UV-detector 290 nm. [**2**]Cl_2, ESI-MS: (calc. *m/z* for $[\mathbf{2}]^{2+}$ = 565.7 and $[\mathbf{2}]^{3+}$ = 377.1), found: 566.0 and 377.4, HPLC (10-90% MeCN/H_2O with 0.1% TFA, 20 min): t_R = 9.9 min.

2.5.1.5 [Ru(Ph$_2$phen)$_2$(Ac-HRGDH-NH$_2$)]Cl$_2$ ([3]Cl$_2$)

cis-Ru(Ph$_2$phen)$_2$Cl$_2$ (0.05 mmol, 41.8 mg) was added to a 2-neck 25 ml flask, the flask was vacuum-flushed with N_2 3 times, deoxygenated MilliQ H_2O (3 mL) was added and the ruthenium solution was stirred at 90°C for 10 min. The peptide powder Ac-HRGDH-NH_2 (0.05mmol, 33 mg) was dissolved in MilliQ water (3 mL) and the pH adjusted to 7.5 by 0.5 mM and 0.1 mM NaOH and HCl solution. The peptide solution was deaerated by bubbling N_2 for 10 min and then injected to the reaction flask . The mixture was then stirred at 90°C for 1 day. After that, the solution was cooled down to room temperature and lyophilized, to afford a reddish powder. Further purification was accomplished by HPLC. The purification were realized by a 250 x 21.2 mm Jupiter® 4 µm Proteo 90 Å C12 column using Thermo Scientific UHPLC system. The gradient was controlled by four pump. Mobile phase consisted H_2O containing 0.1% v/v Trifluoroacetic acid (TFA) (A phase) and acetonitrile containing 0.1% v/v Trifluoroacetic acid (TFA) (B phase). The gradient for **[3]Cl$_2$** preparative separation was 30-

40% MeCN/H_2O for 20 min. The analysts were monitored by four UV detector (214 nm, 290 nm, 350 nm, 450 nm) and the flow rate was 14 mL/min. Compound were collected at UV-detector 290 nm. [**3**]Cl_2, ESI-MS: (calc. *m/z* for $[\mathbf{3}]^{2+}$ = 713.7 and $[\mathbf{3}]^{3+}$ = 475.8), found: 713.5 and 475.7, HPLC (10-90% MeCN/H_2O with 0.1% TFA, 20 min): t_R = 15.0 min.

2.5.2 Photochemistry study

2.5.2.1 UV-vis spectroscopy

UV-vis spectroscopy was performed using a Cary 60 spectrometer from Varian equipped with a Peletier temperature control set to 25°C and a magnetic stirrer. Experiments were performed in a 1 cm optical pathlength quartz cuvette containing 3 mL of solution. The desired complex was prepared using MilliQ water or acetonitrile to a certain concentration. When the experiment was carried out, the sample was deaerated for 15 min by gentle N_2 bubbling on top of the cuvette. A 515 nm green LED light source was fitted on the top of the cuvette with a cooling system, and light was turned on after 1 spectrum measurement. The irradiation beam was vertical (optical pathlength 3 cm), and the measurement beam was horizontal (optical pathlength 1 cm). Standard measurement method: every 30 s for the first 10 min, then every 1 min for the next 10 min, and finally every 10 min until the end of the experiment (120 min).

2.5.2.2 Emission spectroscopy

The emission spectra of the complexes were obtained via a FLS900 spectrometer from Edinburgh Instruments Ltd. Experiments were performed in a 1 cm quartz cuvette containing 0.5 mL of solution at 25 °C. The desired complex was prepared using MilliQ water to final concentration (80 µM). All solutions were measured using λ_{exc}=480 nm, and an emission window of 500-900 nm. Working solutions were irradiated with 515 nm LED green light and emission spectroscopy was measured at irradiation times 0, 10, 20, 30, 60 and 120 min).

2.5.2.3 Singlet oxygen generation

Singlet oxygen quantum yield measurements were performed by direct spectroscopic detection of the 1275 nm emission in CD_3OD, as described by Meijer *et al*.[37]

2.5.3 Uptake study by ICP-MS

A549 cells (5000) and MCF7 cells (8000) were seeded in 96-well plates, each well contained 100 µL Opti-MEM (Gibco complete medium supplemented with 2.5% v/v fetal calf serum (FCS), 0.2% v/v penicillin/streptomycin (P/S), and 1% v/v glutamine). After 24 h, 20 µM of compound [**1**]Cl_2, [**2**]Cl_2,[**3**]Cl_2, $[Ru(bpy)_3]Cl_2$ or $[Ru(Ph_2phen)_2(bpy)]Cl_2$ dissolved in Opti-

MEM were added to each well and the plates were put in a normoxic incubator (21% O_2) for 24 h. After that, the drug-containing medium was removed and every well was washed by drug-free PBS buffer once. Cells were then stained by Nuclear Blue (Invitrogen, R37605) for 30 min. After refreshing by Opti-MEM medium, the wells were imaged by a Nikon TiE2000 confocal laser microscope. The cell number of each well was analyzed by Image-Pro Analyzer 7.0. Then, the medium was then removed and cells were digested by adding 100 µL of 65% HNO_3 for 30 min at room temperature. The cell lysates were transferred to a deep well plate (Eppendorf, E951033502) and diluted with 0.9 mL MilliQ water. The ruthenium concentration in each well was measured in ppb using ICP-MS (NexION 2000, PerkinElmer). Combining the cell numbers and Ru uptake (ppb), calculating the averages and errors from sextuplicate wells, the ruthenium uptake values were finally expressed in µg Ru/million cells.

2.5.4 Colocalization study by Confocal Laser Scanning Microscopy (CLSM)

A549 cells (2×10^4) were seeded in Opti-MEM to 8-well chamber slide (Ibidi, µ-Slide 80827), grown in Opti-MEM medium in the dark for 24 h, treated with compound [**1**]Cl_2 (100 µM) or [**3**]Cl_2 (20 µM), respectively. After incubation for 3 h, the cells were refreshed and then incubated with Nuclear Blue (Fischer scientific, 2 drops/ml, incubated for 10 min, Ref: R37605) and Mito Tracker green (Fischer scientific, 20 nM, Ref: M7514), Golgi Tracker green (Fischer scientific, 20 nM, Ref: B22650) and LysoTracker green (Fischer scientific, 100 nM, Ref: L7526) dyes for 60 min at 37 °C. Before imaging, all dyes were removed (without washing) and cells were covered with 200 µL fresh Opti-MEM. Confocal Laser Scanning Microscopy (CLSM) images were captured using a Leica SP8 microscope (75×, 0.75D) and processed using *NIS* Elements software. The fluorescence intensity profile plots were generated using Fiji ImageJ software. [**1**]Cl_2 and [**3**]Cl_2 were excited at 488 nm and emission was recorded in the 649-796 nm window. Hoechst was excited at 405 nm and emission was detected between 410-490 nm. Mito Tracker green, Golgi Tracker green, and Lyso Tracker green were excited at 488 nm and their emission was captured between 500-597 nm. The Pearson correlation coefficients values were calculated using Fiji imageJ software.

2.6 References

1. B. Englinger, C. Pirker, P. Heffeter, A. Terenzi, C. R. Kowol, B. K. Keppler and W. Berger, *Chemical reviews*, 2018, **119**, 1519-1624.
2. S. Campagna, F. Puntoriero, F. Nastasi, G. Bergamini and V. Balzani, *Photochemistry and Photophysics of Coordination Compounds I*, 2007, 117-214.
3. F. E. Poynton, S. A. Bright, S. Blasco, D. C. Williams, J. M. Kelly and T. Gunnlaugsson, *Chemical Society Reviews*, 2017, **46**, 7706-7756.
4. A. Grzybowski, J. Sak and J. Pawlikowski, *Clinics in Dermatology*, 2016, **34**, 532-537.
5. B. S. Howerton, D. K. Heidary and E. C. Glazer, *Journal of the American Chemical Society*, 2012, **134**, 8324-8327.

6. C. A. Robertson, D. H. Evans and H. Abrahamse, *Journal of Photochemistry and Photobiology B: Biology*, 2009, **96**, 1-8.
7. J. M. Dąbrowski, in *Advances in Inorganic Chemistry*, Elsevier, 2017, vol. 70, pp. 343-394.
8. H. D. Cole, J. A. Roque III, G. Shi, L. M. Lifshits, E. Ramasamy, P. C. Barrett, R. O. Hodges, C. G. Cameron and S. A. McFarland, *Journal of the American Chemical Society*, 2021.
9. L. N. Lameijer, D. Ernst, S. L. Hopkins, M. S. Meijer, S. H. Askes, S. E. Le Dévédec and S. Bonnet, *Angewandte Chemie*, 2017, **129**, 11707-11711.
10. V. H. van Rixel, V. Ramu, A. B. Auyeung, N. Beztsinna, D. Y. Leger, L. N. Lameijer, S. T. Hilt, S. E. Le Dévédec, T. Yildiz and T. Betancourt, *Journal of the American Chemical Society*, 2019, **141**, 18444-18454.
11. A. N. Hidayatullah, E. Wachter, D. K. Heidary, S. Parkin and E. C. Glazer, *Inorganic chemistry*, 2014, **53**, 10030-10032.
12. J. D. Knoll, B. A. Albani, C. B. Durr and C. Turro, *The Journal of Physical Chemistry A*, 2014, **118**, 10603-10610.
13. R. N. Garner, L. E. Joyce and C. Turro, *Inorganic Chemistry*, 2011, **50**, 4384-4391.
14. J. F. Machado, J. D. Correia and T. S. Morais, *Molecules*, 2021, **26**, 3153.
15. F. Danhier, A. Le Breton and V. r. Préat, *Molecular pharmaceutics*, 2012, **9**, 2961-2973.
16. A. L. Dunehoo, M. Anderson, S. Majumdar, N. Kobayashi, C. Berkland and T. J. Siahaan, *Journal of pharmaceutical sciences*, 2006, **95**, 1856-1872.
17. B. LaFoya, J. A. Munroe, A. Miyamoto, M. A. Detweiler, J. J. Crow, T. Gazdik and A. R. Albig, *International journal of molecular sciences*, 2018, **19**, 449.
18. R. O. Hynes, *Matrix biology: journal of the International Society for Matrix Biology*, 2004, **23**, 333.
19. F. Danhier, A. Le Breton and V. Préat, *Molecular Pharmaceutics*, 2012, **9**, 2961-2973.
20. R. J. Hatley, S. J. Macdonald, R. J. Slack, J. Le, S. B. Ludbrook and P. T. Lukey, *Angewandte Chemie International Edition*, 2018, **57**, 3298-3321.
21. J. A. Cuellogaribo, M. S. Meijer and S. Bonnet, *Chemical Communications*, 2017, 6768-6771.
22. X. Ma, J. Jia, R. Cao, X. Wang and H. Fei, *Journal of the American Chemical Society*, 2014, **136**, 17734-17737.
23. S. Bogdanowich-Knipp, D. Jois and T. Siahaan, *The Journal of peptide research*, 1999, **53**, 523-529.
24. C. S. Burke, A. Byrne and T. E. Keyes, *Journal of the American Chemical Society*, 2018, **140**, 6945-6955.
25. C. S. Burke, A. Byrne and T. E. Keyes, *Angewandte Chemie International Edition*, 2018, **57**, 12420-12424.
26. F. Barragán, P. López-Senín, L. Salassa, S. Betanzos-Lara, A. Habtemariam, V. Moreno, P. J. Sadler and V. Marchán, *Journal of the American Chemical Society*, 2011, **133**, 14098-14108.
27. E. Hahn, N. Estrada-Ortiz, J. Han, V. F. Ferreira, T. Kapp, J. D. Correia, A. Casini and F. E. Kühn, *European Journal of Inorganic Chemistry*, 2017, **2017**, 1667-1672.
28. J. Mosquera, M. I. Sánchez, J. L. Mascareñas and M. E. Vázquez, *Chemical Communications*, 2015, **51**, 5501-5504.
29. R. Gulka and S. S. Isied, *Inorganic Chemistry*, 1980, **19**, 2842-2844.
30. A. N. Hidayatullah, E. Wachter, D. K. Heidary, S. Parkin and E. C. Glazer, *Inorganic Chemistry*, 2014, **53**, 10030.
31. A. C. Laemmel, J. P. Collin and J. P. Sauvage, *European journal of inorganic chemistry*, 1999, **1999**, 383-386.
32. K. Graham and E. Unger, *International journal of nanomedicine*, 2018, **13**, 6049.
33. J. Dang, H. He, D. Chen and L. Yin, *Biomaterials science*, 2017, **5**, 1500-1511.
34. D. E. Dolmans, D. Fukumura and R. K. Jain, *Nature reviews cancer*, 2003, **3**, 380-387.
35. V. Van Rixel, B. Siewert, S. Hopkins, S. Askes, A. Busemann, M. Siegler and S. Bonnet, *Chemical science*, 2016, **7**, 4922-4929.
36. S. Bonnet, *Dalton Transactions*, 2018, **47**, 10330-10343.
37. M. S. Meijer and S. Bonnet, *Inorganic chemistry*, 2019, **58**, 11689-11698.
38. T. Zako, H. Nagata, N. Terada, A. Utsumi, M. Sakono, M. Yohda, H. Ueda, K. Soga and M. Maeda, *Biochemical and biophysical research communications*, 2009, **381**, 54-58.
39. S. E. Ackerman, C. M. Wilson, S. A. Kahn, J. R. Kintzing, D. A. Jindal, S. H. Cheshier, G. A. Grant and J. R. Cochran, *Cureus*, 2014, **6**.
40. A. Iannello and A. Ahmad, *Cancer and Metastasis Reviews*, 2005, **24**, 487-499.
41. T. A. Waldmann, *Science*, 1991, **252**, 1657-1662.
42. J.-A. Cuello-Garibo, M. S. Meijer and S. Bonnet, *Chemical Communications*, 2017, **53**, 6768-6771.